

MEMORY EFFICIENT TRANSFORMER ADAPTER FOR DENSE PREDICTIONS

Dong Zhang^{1,2}, Rui Yan³, Pingcheng Dong¹, Kwang-Ting Cheng¹

¹The Hong Kong University of Science and Technology

²InnoHK AI Chip Center for Smart Emerging Systems, ³Nanjing University

{dongz, timcheng}@ust.hk; ruiyan@nju.edu.cn; pingcheng.dong@connect.ust.hk

ABSTRACT

While current Vision Transformer (ViT) adapter methods have shown promising accuracy, their inference speed is implicitly hindered by inefficient memory access operations, *e.g.*, standard normalization and frequent reshaping. In this work, we propose META, a simple and fast ViT adapter that can improve the model’s memory efficiency and decrease memory time consumption by reducing the inefficient memory access operations. Our method features a memory-efficient adapter block that enables the common sharing of layer normalization between the self-attention and feed-forward network layers, thereby reducing the model’s reliance on *normalization operations*. Within the proposed block, the cross-shaped self-attention is employed to reduce the model’s frequent *reshaping operations*. Moreover, we augment the adapter block with a lightweight convolutional branch that can enhance local inductive biases, particularly beneficial for the dense prediction tasks, *e.g.*, object detection, instance segmentation, and semantic segmentation. The adapter block is finally formulated in a cascaded manner to compute diverse head features, thereby enriching the variety of feature representations. Empirically, extensive evaluations on multiple representative datasets validate that META substantially enhances the predicted quality, while achieving a new state-of-the-art accuracy-efficiency trade-off. Theoretically, we demonstrate that META exhibits superior generalization capability and stronger adaptability.

1 INTRODUCTION

State-of-the-art computer vision models typically follow the intuitive paradigm of pre-training on large single-modal general datasets, followed by fine-tuning on local task-specific datasets to achieve promising accuracy (Chen et al., 2021; Zhang et al., 2024; Radford et al., 2021; He et al., 2022; Zhang et al., 2023). However, this defacto paradigm requires downstream models to load the entire pre-trained model for fine-tuning, which may result in several undesirable drawbacks such as poor structural flexibility, large optimization gaps, and limited applicability in certain scenarios (Jie & Deng, 2023; Du et al., 2022; Jie & Deng, 2022). More importantly, these drawbacks have become more prominent and urgent problems that need to be addressed for dense prediction tasks, particularly in the current context of significant model size growth (Gao et al., 2023; Zhang et al., 2022c; Radford et al., 2021; Zhang et al., 2023; Kirillov et al., 2023).

Recently, with the increasing dominance of Vision Transformer (ViT) architectures (Han et al., 2022; Liu et al., 2021; Khan et al., 2022), following the parameter-efficient transfer learning mechanism (Houlsby et al., 2019), ViT adapter has become a central approach to learning vision-specific inductive biases from pre-trained ViT models (Hu et al., 2022; Jie & Deng, 2023; Chen et al., 2022b; Ma et al., 2024; Luo et al., 2023; Shao et al., 2024), successfully addressing the drawbacks associated with the pre-training followed by fine-tuning paradigm. The progressive ViT adapter enables downstream ViT models to achieve promising accuracy levels that are comparable to, or even higher than, those achieved by fine-tuning the entire model. In particular, thanks to the utilization of plain ViT models, which contain unique multi-modal information, adapters based on these models can effectively promote downstream models to learn beneficial semantic-rich feature representations (Touvron et al., 2021; Hu et al., 2022; Kirillov et al., 2023; Dosovitskiy et al., 2020). For example, ViT adapter under the plain ViT models has been successfully applied in multiple computer vision tasks,

e.g., object detection (ODet) (Li et al., 2022b), instance segmentation (ISeg) (Liu et al., 2024), and semantic segmentation (SSeg) (Xie et al., 2021).

Despite the significant progress made by existing ViT adapters (Chen et al., 2022b; Liu et al., 2024; Jie & Deng, 2023; Marouf et al., 2024), their inference speed is still somewhat unfavorable, which limits their implementations on edge computing devices (Dong et al., 2024a) and applications for real-time recognition scenarios (Marouf et al., 2024). Recently, it has been revealed that in addition to computation and parameter complexity (*e.g.*, FLOPs and #Params.), inefficient memory access operations (Marouf et al., 2024; Liu et al., 2023), such as standard normalization and frequent reshaping operations, play a critical role in hindering the ViT’s inference speed (He & Hofmann, 2024; Pan et al., 2022; Fournier et al., 2023; Shi et al., 2023). In other words, the inefficient planning of memory access may cause delays and prevent models from fully utilizing the computing power of GPUs or CPUs, resulting in a significant negative impact on the speed of ViT models (Liu et al., 2023; Dao et al., 2022; Venkat et al., 2019; Gu et al., 2021; Ivanov et al., 2021). However, these inefficient memory access operations are usually overlooked factors during the network design process for dense prediction tasks. In this work, we explore how to solve this problem and accelerate the inference speed of ViT adapters in downstream models. *Our solution is to decrease memory time consumption by reducing layer normalization and frequent reshaping operations.*

We propose a simple and fast memory efficient transformer adapter (META) that can improve the model’s memory efficiency and decrease memory time consumption by reducing the inefficient memory access operations. As illustrated in Figure 1, our META demonstrates advantages over existing ViT models and ViT adapters in terms of memory consumptions and inference time costs.

	ViT	ViT Adapter	META(Ours)
Training Params.	☒ High	☑ Low	☑ Low
Application gaps	☒ High	☑ Low	☑ Low
Memory consumptions	☒ High	☒ High	☑ Low
Inference time costs	☒ High	☒ High	☑ Low

Figure 1: Qualitative performance comparisons of different models with respect to training parameters, application gaps, memory access costs, and inference time costs.

The main contribution of this work is the proposal of a *memory-efficient adapter block* that shares normalization operations between the self-attention and feed-forward network layers, which exist in a parallel manner (Ref. Sec. 3.2). Within this block, the cross-shaped self-attention is employed to reduce the reliance for frequent reshaping operations. Consequently, the proposed two reverse designs are capable of significantly reducing the memory consumption of the ViT adapter, resulting in an improved inference speed. Moreover, to enrich local inductive biases for dense predictions, a *lightweight convolutional branch* is introduced into the *memory-efficient adapter block*. In the process of interacting with the ViT backbone, a *cascaded mechanism* is further proposed to compute different head features, which can enhance the diversity of the obtained feature representations. We conduct extensive experiments for ODet, ISeg and SSeg on two challenging datasets, namely MSCOCO (Lin et al., 2014) and ADE20K (Zhou et al., 2017), for evaluating our META. The obtained results demonstrate that META substantially enhances prediction quality, attains a new state-of-the-art accuracy level, reduces the number of parameters and memory consumption requirements, and achieves faster inference speeds. Theoretically, we also prove that META can exhibit superior generalization capability and stronger adaptability compared to existing ViT adapter methods¹.

2 RELATED WORK

Vision Transformer (ViT). Current ViT models for state-of-the-art computer vision tasks can be roughly divided into two camps: *plain ViT models*, which are designed to learn general vision features (*e.g.*, ViT (Dosovitskiy et al., 2020), DeiT (Touvron et al., 2021) and TDE Transformer (Touvron et al., 2021)), and *hierarchical ViT models*, which are designed to learn vision-specific features (*e.g.*, Swin Transformer (Liu et al., 2021) and PVT (Wang et al., 2021b)). Both camps of ViT models have their pros and cons. For example, the *hierarchical ViT models* can learn powerful vision-specific feature representations, which makes them usually perform better than the *plain ViT models* on accuracy (Han et al., 2022; Khan et al., 2022; Kirillov et al., 2023). However, their unvarnished disadvantage is the lack of multi-modal pre-training information for dense predictions (Chen et al., 2022b). On the other hand, although the *plain ViT models* have weak prior assumptions, which results in lower accuracy compared to the *hierarchical ViT models*, their multi-modal pre-training in-

¹Due to page limitations, the theoretical analysis will be provided in the supplementary materials.

formation has great potential to provide semantic-rich feature representations for downstream models (Guo et al., 2022; Zhang et al., 2023; He et al., 2022; Zhang et al., 2024; Jia et al., 2022). In this paper, we focus on the *plain ViT models* for dense predictions. Our contribution is the proposal of a straightforward and memory efficient ViT adapter, starting from the reduction of inefficient memory access operations.

ViT for Dense Predictions. Dense predictions, including ODet, ISeg, and SSeg, aim at predicting a semantic mask where each pixel/object in the given image is assigned a class label (Ranftl et al., 2021; Zhang et al., 2023; Vandenhende et al., 2021). For ISeg, the obtained mask also distinguishes different objects of the same class. With the development of ViT technologies, dense prediction models based on ViT have become one of the default choices for state-of-the-art methods (Liu et al., 2021; Wang et al., 2021b; Dosovitskiy et al., 2020). These methods can be mainly divided into two categories: those based on Transformers and those that incorporate a combination of CNN layers. The former, *e.g.*, SegFormer (Strudel et al., 2021), HRViT (Gu et al., 2022), Segvit (Zhang et al., 2022a), Swin UNet (Hatamizadeh et al., 2021), and ISTR (Hu et al., 2021), extract features from a given image and connect with task-specific head networks to achieve specific recognition purposes. The latter compensates for the lack of local inductive bias in the pure ViT architecture by introducing local convolutional layers, and representative methods include ConFormer (Peng et al., 2021), CVT (Wu et al., 2021), NextViT (Li et al., 2022a), and CAE-GReaT (Zhang et al., 2023). While the former can capture long-range dependencies and achieve favorable recognition capability, they require sufficient training samples to optimize the model, and further improvement is needed on memory access and inference speed. To this end, we propose a solution to the problem of limited inference speed caused by frequent memory consumption using a pre-trained ViT model.

ViT Adapters. Adapter methods are originally derived from the NLP tasks, such as PALs (Stickland & Murray, 2019) and NLP adapter (Houlsby et al., 2019). These methods add a small number of trainable modules to a pre-trained network, so that downstream fine-tuning models can quickly adapt to specific datasets and tasks via a parameter-efficient transfer learning manner (Hu et al., 2022; Houlsby et al., 2019; Chen et al., 2022b; Shen et al., 2023). In the computer vision domain, ViT adapters have also adopted the similar paradigm (Jie & Deng, 2023; Chen et al., 2022b; Shao et al., 2024; Luo et al., 2023). ViT adapter method is used to fine-tune large-scale plain ViT models with a small number of trainable parameters and achieve promising accuracy (Jie & Deng, 2023; Li et al., 2022b; Chen et al., 2022b). Inspired by (He & Hofmann, 2024; Jie & Deng, 2022; Chen et al., 2022b; Liu et al., 2023; Mercea et al., 2024), we propose an efficient solution to enhance the memory efficiency and minimize memory time consumption of ViT adapters. We also provide theoretical analysis to demonstrate the superior generalization and adaptability of our method.

3 MEMORY EFFICIENT TRANSFORMER ADAPTER (META)

3.1 OVERALL ARCHITECTURE AND CONFIGURATIONS

As illustrated in Figure 2, the network takes an arbitrary RGB image $\mathbf{I} \in \mathbb{R}^{H \times W \times 3}$ as input and predicts a semantic mask $\mathbf{O} \in \mathbb{R}^{H \times W \times C}$ as output. H and W denotes the image height and width, respectively, and C denotes the class size of the used dataset. Following (Jie & Deng, 2023; Li et al., 2022b; Chen et al., 2022b), the whole network mainly consists of two parts: the upper part is a pre-trained plain ViT model (*e.g.*, ViT (Li et al., 2021)), which consists of 4 blocks. The i -th ($i = 1, 2, 3, 4$) block contains a set of semantic features \mathbf{F}_{vit}^i with the spatial size of $1/4, 1/8, 1/16$, and $1/32$ of \mathbf{I} , respectively. The lower part is a trainable ViT adapter, which includes a spatial prior module as in (Chen et al., 2022b) for \mathbf{I} 's encoding, where the encoded features within each block denote \mathbf{F}_{sp}^i , as well as a set of cascaded memory efficient adapter (MEA) injectors (Ref. Sec. 3.3) and cascaded MEA extractors (Ref. Sec. 3.4) that act on each ViT backbone block. The ‘‘cascaded’’ refers to a computational scheme that is incorporated into the different heads of the proposed injectors/extractors, which can enhance the diversity of the obtained feature representations. Concretely, for the i -th trainable MEA injector, it injects the updated task-specific features back into the i -th ViT block and into the i -th extractor (as shown in Figure 2 (b)). For the i -th trainable MEA extractor, it extracts the i -th general features for the $(i + 1)$ -th injector (as shown in Figure 2 (c)). This process is repeated until the final ViT block is reached. Due to the incorporation of strategies aimed at reducing inefficient memory access operations in our method, which exhibits enhanced memory efficiency and reduced memory time consumption compared to existing ViT adapters, consequently

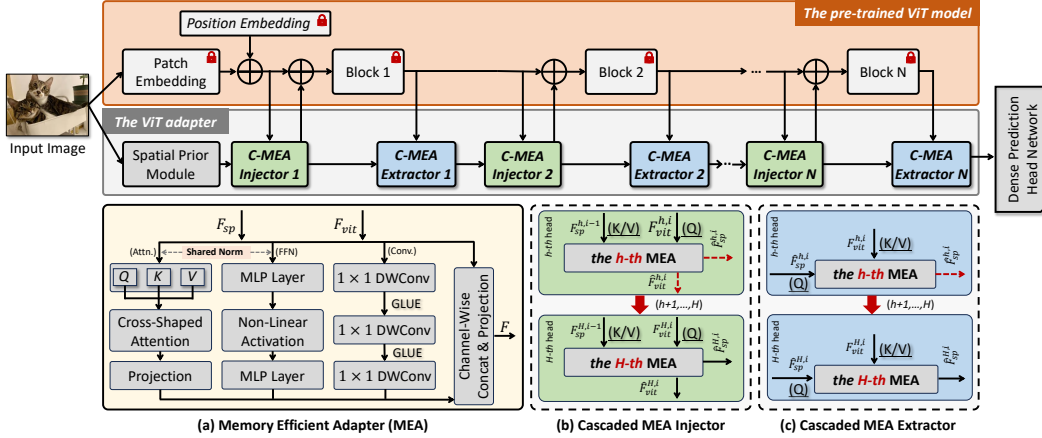


Figure 2: Overall architecture of META. Our primary contribution is the proposal of a MEA block in (a), which serves as the fundamental component for the injector in (b) and extractor in (c).

leading to accelerated inference speed. We will provide a detailed explanation of the basic component and mechanism of the MEA block in the following Sec. 3.2 and how it can be deployed in the MEA injectors and MEA extractors to form a cascaded scheme.

3.2 MEA BLOCK

The MEA block aims to interact the features extracted from the ViT backbone and the spatial prior module. Our block consists of the attention (*i.e.*, Attn) branch, the feed-forward network (*i.e.*, FFN) branch, and the lightweight convolutional (*i.e.*, Conv) branch. The three branches exist in a parallel form, which is beneficial for computing in GPUs. As shown in Figure 2 (a), consider an arbitrary block, the input is \mathbf{F}_{sp} and \mathbf{F}_{vit} , and the output \mathbf{F} is obtained by concatenating the features from the Attn, FFN, and Conv branches along the channel dimension, and then passing them through a feature projection layer. Therefore, this process can be formulated as:

$$\mathbf{F} = \text{Conv}_{3 \times 3}(\text{Concat}(\underbrace{\mathbf{A}(\mathbf{F}_{sp}, \mathbf{F}_{vit})}_{\text{Attn Branch}}, \underbrace{\mathbf{F}(\mathbf{F}_{sp}, \mathbf{F}_{vit})}_{\text{FFN Branch}}, \underbrace{\mathbf{C}(\mathbf{F}_{sp}, \mathbf{F}_{vit})}_{\text{Conv Branch}}; \mathbf{F}_{sp}; \mathbf{F}_{vit})), \quad (1)$$

where $\mathbf{A}(\cdot)$, $\mathbf{F}(\cdot)$, and $\mathbf{C}(\cdot)$ denote the operation of the Attn, FFN, and Conv branch, respectively. In MEA, these three branches exist in a parallel manner. $\text{Concat}(\cdot)$ denotes the feature concatenation operation along the channel dimension, and $\text{Conv}_{3 \times 3}(\cdot)$ denotes a 3×3 convolution with the output channel size of 256 for feature projection. In particular, to construct an memory efficient block, following (He & Hofmann, 2024; Wang & Komatsuzaki, 2021), the Attn and FFN branches are subjected to a shared layer normalization operation, which leads to a decrease in memory time consumption associated with the normalization operations.

Attn Branch. In our work, we adopt the cross-shaped self-attention (CSA) to reduce the model’s access to the memory unit, which allows for the computation of the attention matrix across different spatial dimensions without requiring the input tensor to be frequently reshaped (Dong et al., 2022; Tu et al., 2022). Specifically, CSA first performs self-attention separately along the horizontal and vertical dimensions of the given features. The outputs $\mathbf{A}_H(\mathbf{F}_{sp}, \mathbf{F}_{vit})$ and $\mathbf{A}_V(\mathbf{F}_{sp}, \mathbf{F}_{vit})$ of these two parallel groups are then concatenated along the channel dimension, followed by a feature projection operation via a 3×3 convolution with the output channel size of 256, to form the output $\mathbf{A}(\mathbf{F}_{sp}, \mathbf{F}_{vit})$. For the horizontal self-attention, the input features \mathbf{F}_{sp} and \mathbf{F}_{vit} are first subjected to the shared layer normalization, and then divided into M non-overlapping horizontal stripes, where each stripe has the spatial size of $s \times W$ (*i.e.*, $s = H/M$). Then, the self-attention (Vaswani et al., 2017) is performed on each stripe, which can be formulated as:

$$\mathbf{A}_H^m(\mathbf{F}_{sp}, \mathbf{F}_{vit}) = \text{SA}(\text{LN}(\mathbf{F}_{sp}^m W^Q), \text{LN}(\mathbf{F}_{vit}^m W^K), \text{LN}(\mathbf{F}_{vit}^m W^V)), \quad (2)$$

where $\text{LN}(\cdot)$ denotes the shared layer normalization operation. $\text{SA}(\cdot)$ denotes the classical single head self-attention (Vaswani et al., 2017). m denotes the m -th stripe and $m = 1, 2, \dots, M$. W^Q , W^K , and W^V are used to project the input features into the queries, keys, and values spaces, respectively. The sub-attention results of different stripes are merged together to form the output

$A_H(\mathbf{F}_{sp}, \mathbf{F}_{vit})$ of the horizontal group. In equation 2, we choose \mathbf{F}_{sp} as queries and \mathbf{F}_{vit} as keys and values for the sake of example. In our injector and extractor in Sec 3.3 and Sec 3.4, the roles of \mathbf{F}_{sp} and \mathbf{F}_{vit} can be swapped depending on the specific requirements. The attention computation along the vertical dimension $A_V(\mathbf{F}_{sp}, \mathbf{F}_{vit})$ is also performed in a similar fashion.

FFN Branch. Following the common setting (Vaswani et al., 2017; Tolstikhin et al., 2021), to enable interaction between the obtained features in the channel dimension, our FFN branch consists of two MLP layers and a non-linear activation layer (Saxe et al., 2013; He & Hofmann, 2024), where the MLP layer consists of a sequential arrangement of two 3×3 convolutional layers.

The input of the FFN branch is \mathbf{F}_{sp} and \mathbf{F}_{vit} , which are sequentially processed by feature concatenation along the channel dimension, a 3×3 convolution with the output channel size of 256, and the shared layer normalization. This process can be expressed as:

$$F(\mathbf{F}_{sp}, \mathbf{F}_{vit})_{\text{Tem}} = \text{LN}(\text{Conv}_{3 \times 3}(\text{Concat}(\mathbf{F}_{sp}; \mathbf{F}_{vit}))). \quad (3)$$

The temporary $F(\mathbf{F}_{sp}, \mathbf{F}_{vit})_{\text{Tem}}$ are then passed through a MLP layer, a non-linear activation layer (Saxe et al., 2013), and another MLP layer to obtain the output $F(\mathbf{F}_{sp}, \mathbf{F}_{vit})$. Hence, this can be expressed as:

$$F(\mathbf{F}_{sp}, \mathbf{F}_{vit}) = \text{MLP}(\text{NLA}(\text{MLP}(F(\mathbf{F}_{sp}, \mathbf{F}_{vit})_{\text{Tem}}))), \quad (4)$$

where $\text{MLP}(\cdot)$ denotes the MLP layer operation, and $\text{NLA}(\cdot)$ denotes the non-linear activation layer (Saxe et al., 2013; He & Hofmann, 2024).

Conv Branch. Empirical evidence has demonstrated that incorporating local inductive biases into ViT models can provide notable benefits for visual tasks involving dense prediction (Peng et al., 2021; Wu et al., 2021; Li et al., 2022a; Zhang et al., 2023). To achieve this goal, we introduce a lightweight convolutional branch into the ViT adapter. Specifically, the Conv branch also takes into \mathbf{F}_{sp} and \mathbf{F}_{vit} as the input, which consists of three 1×1 depth-wise convolutions concatenated in series, with a GLUE layer used to activate the features between every two convolutions (Saxe et al., 2013; He & Hofmann, 2024). The computation process of the Conv branch is formulated as:

$$C(\mathbf{F}_{sp}, \mathbf{F}_{vit}) = \text{DC}(\text{GLU}(\text{DC}(\text{GLU}(\text{DC}(\text{Concat}(\mathbf{F}_{sp}; \mathbf{F}_{vit})))))), \quad (5)$$

where $\text{DC}(\cdot)$ denotes the 1×1 depth-wise convolution with the output channel size of 256, and $\text{GLU}(\cdot)$ denotes the GLUE layer. With the help of shared layer normalization and CSA, MEA becomes a memory-efficient module with rich local inductive biases. In the following sections, we will provide detailed instructions on how to deploy our MEA block on injectors and extractors.

3.3 CASCADED MEA INJECTOR

As illustrated in Figure 2 (b), the cascaded MEA injector adopts the paradigm of self-attention in its computational process, where \mathbf{F}_{vit}^i is used as the query, and \mathbf{F}_{sp}^{i-1} generated by the last extractor is used as the key and value. Particularly, to enhance the diversity of the obtained attention maps, a cascaded mechanism is proposed to compute different head features in the cascaded MEA injector. Specifically, we first divide the given features into H parts along the channel dimension in a multi-head manner, following the classic self-attention (Vaswani et al., 2017), where H is set to 16 in our work. In the computation process of each head, the output of the h -th head $\hat{\mathbf{F}}_{sp}^{h,i}$ and $\hat{\mathbf{F}}_{vit}^{h,i}$ is added into the input features of the next $(h+1)$ -th head $\mathbf{F}_{sp}^{h+1,i-1}$ and $\mathbf{F}_{vit}^{h+1,i}$ to be used in the calculation of subsequent self-attention features, where $h = 1, 2, \dots, H$. The cascaded process continues until the feature from the last head is included in the computation. Finally, the features obtained from these heads are concatenated along the channel dimension and projected through a 3×3 convolution layer before being outputted as the output of the i -th cascaded MEA injector. Besides, since the MEA block has only one output, $\hat{\mathbf{F}}_{sp}^{h,i} = \hat{\mathbf{F}}_{vit}^{h,i}$ in our cascaded MEA injector.

3.4 CASCADED MEA EXTRACTOR

As illustrated in Figure 2 (c), following (Marouf et al., 2024; Chen et al., 2022a; Dong et al., 2024b), our i -th cascaded MEA extractor of the h -th head takes the $\hat{\mathbf{F}}_{sp}^{h,i}$ generated by the injector and $\mathbf{F}_{vit}^{h,i}$ as input, where $\hat{\mathbf{F}}_{sp}^{h,i}$ is used as the query, $\mathbf{F}_{vit}^{h,i}$ is used as the key and value. The output of the

i -th cascaded MEA extractor is $\mathbf{F}_{sp}^{h,i}$. Similarly, the cascaded mechanism is applied following the cascaded MEA injector until the feature from the last head is included in the computation.

4 EXPERIMENTS

4.1 DATASETS AND EVALUATION METRICS

Datasets. To facilitate a fair result comparison with existing methods, we conduct experiments, including the ablation analysis, on two commonly used datasets: MS-COCO (Caesar et al., 2018) for ODet and ISeg, and ADE20K (Zhou et al., 2017) for SSeg. Due to page limitations, the implementation details of these datasets will be given in the supplementary materials.

Evaluation metrics. The commonly adopted average precision (AP) and mean intersection-over-union (mIoU) are used to assess the model accuracy for ODet (AP^b)/ISeg (AP^m) and SSeg, respectively. Besides, to evaluate the efficiency, model Parameters (#P), floating point operations (FLOPs), memory consumption (MC) of the adapter, and frames per second (FPS) are also adopted. The reported inference results are measured by A100 GPUs with per-GPU batch size 2.

4.2 EXPERIMENTS ON OBJECT DETECTION (ODET) AND INSTANCE SEGMENTATION (ISEG)

Baselines and settings. As in (Chen et al., 2022b; Xiong et al., 2024; Jie & Deng, 2022; Marouf et al., 2024), Mask R-CNN (He et al., 2017), Cascade Mask R-CNN (Cai & Vasconcelos, 2019), ATSS (Zhang et al., 2020), and GFL (Li et al., 2020) are employed as the baseline models, where the pre-trained ViT (Li et al., 2022b) is used as the backbone. All the baseline models are pre-trained on ImageNet-1k by default (Deng et al., 2009). Unless otherwise specified, these baselines are set up to be consistent with their papers and the settings of the ViT-Adapter (Chen et al., 2022b) method.

Comparisons with state-of-the-art (SOTA) methods. Result comparisons with SOTA methods with Mask R-CNN (He et al., 2017) for ODet and ISeg are shown in Table 1. From this table, we can obtain the following observations and conclusions: *i*) Compared to the experimental results of the Mask R-CNN (He et al., 2017) model with ViT (Li et al., 2021), our proposed META can consistently improve accuracy for ODet and ISeg across different model scales (e.g., ViT-T/S/B/L (Li et al., 2021)), while only adding a small number of training parameters. Even with different training schedules (i.e., 1×, and 3× with MS), our method can also improve the model performance, demonstrating the plug-and-play advantage of META. *ii*) Compared to the SOTA ViT-Adapter (Chen et al., 2022b) and LoSA (Mercea et al., 2024), META can achieve a new accuracy-efficiency trade-off. For example, in settings with the strong ViT-B (Li et al., 2021) as the backbone, our method achieves a performance gain of 0.5%AP^m under 1× training schedule and 0.7%AP^m under 3× training schedule with MS while reducing 4.9M model parameters, when compared to ViT-Adapter (Chen et al., 2022b). *iii*) Even with stronger pre-trained models, META still improves performance on the baseline models and surpasses existing methods on accuracy, parameters and memory. For example, on the ImageNet-22k pre-trained weights from (Steiner et al., 2021), our method achieves a performance gain of 0.8%/0.7%AP^m under 1×/3× training schedule while reducing 8.2M parameters compared to ViT-Adapter (Chen et al., 2022b), which validates its strong learning ability and flexible adaptability. *iv*) Compared to SOTA ODet and ISeg methods, META also has very competitive performance. For example, compared to the strong ViTDet-B (Li et al., 2022b) model, META-T has 2.2%AP^b and 3.1%AP^m gains under the 1× training schedule, and has META-T has 4.9%AP^b and 2.7%AP^m gains under the 3× training schedule. *v*) Compared to SOTA ViT adapter methods such as AdaptFormer (Chen et al., 2022a), FacT-TK (Jie & Deng, 2023), and LoSA (Mercea et al., 2024), our method exhibits superior efficiency in terms of reduced parameter count, decreased FLOPs, and lower MC. Particularly, META only utilizes 62% of the MC of LoSA while achieving superior prediction accuracy. Therefore, the experimental results and conclusions above demonstrate that our method achieves better accuracy and higher efficiency in dense prediction tasks.

Superiority performance under different baselines. In addition to Mask R-CNN, we also choose Cascade Mask R-CNN (Cai & Vasconcelos, 2019), ATSS (Zhang et al., 2020), and GFL (Li et al., 2020) as the baselines as in Chen et al. (2022b); Mercea et al. (2024). We explore the effectiveness and superiority performance of META on these baseline models, where the 3× training with MS

Methods	#P (M)	FLOPs (G)	MC (GB)	1× schedule				3× +MS schedule			
				AP ^b	AP ^m	AP ^m ₅₀	AP ^m ₇₅	AP ^b	AP ^m	AP ^m ₅₀	AP ^m ₇₅
ViT-T (Li et al., 2021)	26.1	205	NA	35.5	33.5	54.9	35.1	44.9	37.0	59.6	39.0
ViTDet-T (Li et al., 2022b)	26.6	209	NA	35.7	33.5	54.7	35.2	40.4	37.1	60.1	39.3
ViT-Adapter-T (Chen et al., 2022b)	28.1	208	15.2	41.1	37.5	59.7	39.9	46.0	41.0	64.4	44.1
AdaptFormer-T (Chen et al., 2022a)	27.9	210	17.7	36.4	34.2	55.6	35.9	45.2	37.5	60.5	40.8
FacT-TK-T (Jie & Deng, 2023)	27.7	213	16.1	36.6	34.5	55.5	36.7	46.3	41.2	64.7	44.0
LoSA-T (Mercea et al., 2024)	27.6	208	13.0	41.4	38.0	60.1	40.5	46.1	39.5	64.2	44.3
META-T (Ours)	27.4	206	8.1	43.1	38.6	60.8	41.1	47.5	41.6	65.0	44.8
ViT-S (Li et al., 2021)	43.8	245	NA	40.2	37.1	59.9	39.3	44.0	39.9	63.4	42.2
ViTDet-S (Li et al., 2022b)	43.8	255	NA	40.6	37.1	60.0	38.8	44.5	40.1	63.6	42.5
ViT-Adapter-S (Chen et al., 2022b)	47.8	251	15.2	44.7	39.9	62.5	42.8	48.2	42.8	66.4	45.9
AdaptFormer-S (Chen et al., 2022a)	47.5	255	17.7	41.2	37.8	60.3	41.0	45.0	41.2	64.2	43.4
FacT-TK-S (Jie & Deng, 2023)	46.8	259	16.1	41.5	37.8	60.7	41.2	45.2	41.8	65.0	42.9
LoSA-S (Mercea et al., 2024)	46.1	249	13.0	44.2	39.8	62.6	42.5	48.3	42.5	66.5	46.0
META-S (Ours)	45.2	247	8.1	45.5	40.5	63.4	43.5	49.5	43.3	66.9	46.6
ViT-B (Li et al., 2021)	113.6	719	NA	42.9	39.4	62.6	42.0	45.8	41.3	65.1	44.4
ViTDet-B (Li et al., 2022b)	121.3	800	NA	43.2	39.2	62.7	41.4	46.3	41.6	65.3	44.5
ViT-Adapter-B (Chen et al., 2022b)	120.2	730	15.2	47.0	41.8	65.1	44.9	49.6	43.6	67.7	46.9
AdaptFormer-B (Chen et al., 2022a)	118.5	733	17.7	44.5	40.3	63.1	43.0	46.2	42.4	66.2	45.7
FacT-TK-B (Jie & Deng, 2023)	118.0	735	16.1	44.9	41.2	64.1	43.2	47.6	43.2	67.5	46.3
LoSA-B (Mercea et al., 2024)	117.2	722	13.0	45.1	41.8	64.6	44.0	48.6	43.8	67.9	47.0
META-B (Ours)	115.3	720	8.1	45.4	42.3	66.0	45.7	51.2	44.3	68.2	47.5
ViT-L [‡] (Li et al., 2021)	337.3	1,907	NA	45.7	41.5	65.6	44.6	48.3	43.4	67.9	46.6
ViTDet-L [‡] (Li et al., 2022b)	350.9	1,900	NA	46.2	41.4	65.8	44.1	49.1	44.0	68.5	47.6
ViT-Adapter-L [‡] (Chen et al., 2022b)	347.9	1,927	15.2	48.7	43.3	67.0	46.9	52.1	46.0	70.5	49.7
AdaptFormer-L [‡] (Chen et al., 2022a)	345.7	1,924	17.7	46.3	42.6	66.1	45.8	49.0	44.8	68.1	47.1
FacT-TK-L [‡] (Jie & Deng, 2023)	342.1	1,925	16.1	46.5	42.9	66.5	46.0	48.8	44.5	68.2	47.0
LoSA-L [‡] (Mercea et al., 2024)	341.3	1,922	13.0	50.2	43.5	66.8	47.1	53.2	46.2	71.0	48.9
META-L[‡] (Ours)	339.7	1,905	8.1	51.8	44.1	67.6	47.8	55.3	46.7	71.3	50.4

Table 1: Result comparisons with SOTA methods under Mask R-CNN (He et al., 2017) on the *val* set of MS-COCO. ‡ denotes the model is pre-trained on ImageNet-22k as in (Steiner et al., 2021). “MS” denotes the multi-scale training strategy. “NA” denotes not applicable.

strategy is used. The experimental results are given in Table 2. We can observe that META can consistently improve performance across different baselines, and exhibits more accurate and more efficient advantages compared to SOTA ViT adapter methods. For example, based on the Cascade Mask R-CNN (Cai & Vasconcelos, 2019), META-S can achieve up to 44.8% AP^m with only 83M parameters, 797G FLOPs, and 8.1GB MC, which is 1.3% AP^m higher, 3M fewer parameters, 4G fewer FLOPs, and 7.1GB fewer MC compared to the competitive ViT-Adapter-T method (Chen et al., 2022b). Besides, META-B can achieve a 1.7% AP^b/0.5% AP^m gain on the 3× training schedule, with 5M fewer parameters and 5G fewer FLOPs than the ViT-Adapter-B (Chen et al., 2022b) model. On ATSS and GFL, our method also achieves competitive 43.2% and 44.0% AP^m, respectively, which are 0.7% and 0.9% AP^m higher than the competitive vision adapter ViT-Adapter-S (Chen et al., 2022b). In terms of efficiency, compare with the SOTA LoSA (Mercea et al., 2024) method, our method has fewer parameters (33M v.s. 35M), fewer FLOPs (265G v.s. 268G under ATSS, 279G v.s. 284G under GFL), and fewer MC (8.1GB v.s. 13.0GB under ATSS and GFL), indicating its higher computation and memory efficiency.

4.3 EXPERIMENTS ON SEMANTIC SEGMENTATION (SSEG)

Baselines and Settings. Following (Chen et al., 2022b; Jie & Deng, 2023; 2022), we select Semantic FPN (Kirillov et al., 2019) and UperNet (Xiao et al., 2018) as baseline models, where the Semantic FPN is trained for 80k iterations and the UperNet is trained for 160k iterations as in (Wang et al., 2021b; Liu et al., 2021). Unless otherwise specified, the training and inference settings are set up to be consistent with the ViT-Adapter (Chen et al., 2022b).

Methods	#P	FLOPs	MC	FPS	AP ^b	AP ^m	AP ^m ₅₀	AP ^m ₇₅
Cascade Mask R-CNN (Cai & Vasconcelos, 2019) 3× +MS schedule								
Swin-T (Liu et al., 2021)	86	745	NA	15.3	50.5	43.7	66.6	47.1
ViT-S (Li et al., 2021)	82	795	NA	16.5	47.9	42.8	62.1	44.8
ViT-Adapter-S (Chen et al., 2022b)	86	801	15.2	13.1	51.5	43.5	63.0	48.2
LoSA-S (Mercea et al., 2024)	84	799	13.0	12.0	53.5	43.8	64.1	48.1
META-S_(Ours)	83	797	8.1	14.7	54.3	44.8	66.8	49.5
Swin-B (Liu et al., 2021)	145	982	NA	11.6	51.9	45.0	68.4	48.7
ViT-B (Li et al., 2021)	151	1,100	NA	13.0	50.1	42.7	63.9	44.1
ViT-Adapter-B (Chen et al., 2022b)	158	1,106	15.2	8.6	52.1	43.6	64.3	45.2
LoSA-B (Mercea et al., 2024)	155	1,104	13.0	9.0	52.6	43.5	63.8	44.7
META-B_(Ours)	153	1,101	8.1	11.9	53.8	44.1	65.2	45.6
ATSS (Zhang et al., 2020) 3× +MS schedule								
Swin-T (Liu et al., 2021)	36	215	NA	17.1	47.2	41.2	54.8	45.5
ViT-S (Li et al., 2021)	32	263	NA	18.0	45.2	40.5	52.0	41.8
ViT-Adapter-S (Chen et al., 2022b)	36	272	15.2	14.2	49.6	42.5	55.1	46.5
LoSA-S (Mercea et al., 2024)	35	268	13.0	16.0	50.3	41.9	54.4	45.0
META-S_(Ours)	33	265	8.1	16.8	54.9	43.2	55.6	47.4
GFL (Li et al., 2020) 3× +MS schedule								
Swin-T (Liu et al., 2021)	36	251	NA	17.5	47.6	40.8	54.2	46.0
ViT-S (Li et al., 2021)	32	275	NA	18.1	46.0	40.2	52.9	45.1
ViT-Adapter-S (Chen et al., 2022b)	36	288	15.2	15.3	50.0	43.1	54.5	47.1
LoSA-S (Mercea et al., 2024)	35	284	13.0	16.2	51.2	43.3	54.7	47.5
META-S_(Ours)	33	279	8.1	17.6	55.6	44.0	55.2	48.5

Table 2: Result comparisons with SOTA methods under Cascade Mask R-CNN (Cai & Vasconcelos, 2019), ATSS (Zhang et al., 2020), and GFL (Li et al., 2020) on the *val* set of MS-COCO.

Comparisons with state-of-the-art methods. We show the SSeg experimental results of META under different settings and compare them with SOTA SSeg methods in Table 3. We can observe that *i*) Our method can consistently improve performance across different baselines, model scales, training strategies, and pre-training weights (including IN-1K, IN-22K, and MM), while having fewer model parameters and memory consumption compared to the advanced ViT-Adapter (Chen et al., 2022b) and LoSA (Mercea et al., 2024) methods. This demonstrates the strong applicability and learning ability of META, which can solve the problem of limited applicability in certain scenarios of downstream models in the traditional pre-training and fine-tuning strategy at the application level. *ii*) Compared to SOTA methods, META also can achieve a new SOTA accuracy-cost trade-off. The parameter from META is only about 0.2% of the overall model parameter count, indicating a minimal impact on the total parameter count. Furthermore, the memory consumption of our method accounts for only 55.14% of the SOTA LoSA (Mercea et al., 2024). *iii*) On larger model scales, META achieves higher efficiency with fewer parameters (*e.g.*, -1.4M on META-T and -4.2M on META-B). This indicates that our method is suitable for fine-tuning large ViT models.

4.4 ABLATION ANALYSIS

In our ablation analysis for ISeg and ODet, we adopt Mask R-CNN (He et al., 2017) under the 3× training schedule with MS as the baseline and report the experimental results on the *val* set of MS-COCO (Caesar et al., 2018), where the ImageNet-1k pre-trained ViT-B (Li et al., 2022b) is used as the backbone. For SSeg, we choose UperNet (Xiao et al., 2018) with 160k iterations as the baseline, where the ImageNet-1k pre-trained ViT-B (Li et al., 2022b) is used as the backbone. We report the single-scale testing results on the *val* set of ADE20K (Zhou et al., 2017). Due to page limitations, we only present the results of the effectiveness of each component in the main paper. Other aspects, such as result comparisons with other variants of ViT adapter methods, will be provided in the supplementary materials as part of the ablation analysis.

Effectiveness of each component. The experimental results of gradually adding META components on the pre-trained ViT-B (Li et al., 2022b) model are shown in Table 4. First, we can observe that directly using the Attn branch as the adapter on the pre-trained ViT-B (Li et al., 2022b) model not only fails to improve performance but also significantly decreases AP^m and AP^b (*i.e.*, from

Methods	Pre-Training	Semantic FPN 80k				UperNet 160k			
		#P	MC	mIoU	mIoU _(w/MS)	#P	MC	mIoU	mIoU _(w/MS)
PVT-Tiny (Wang et al., 2021b)	IN-1k	17.0	NA	36.6	37.3	43.2	NA	38.5	39.0
ViT-T (Li et al., 2021)	IN-1k	10.2	NA	39.4	40.5	34.1	NA	41.7	42.6
ViT-Adapter-T (Chen et al., 2022b)	IN-1k	12.2	14.0	41.7	42.1	36.1	14.0	42.6	43.6
LoSA-T (Mercea et al., 2024)	IN-1k	11.1	10.7	40.8	41.9	36.3	10.7	42.1	43.7
META-T_(Ours)	IN-1k	10.8	5.9	42.2	43.0	35.0	5.9	43.1	44.1
Twins-SVT-S (Chu et al., 2021)	IN-1k	28.3	NA	43.2	44.1	54.4	NA	46.2	47.1
ViT-S (Li et al., 2021)	IN-1k	27.8	NA	44.6	45.8	53.6	NA	44.6	45.7
ViT-Adapter-S (Chen et al., 2022b)	IN-1k	31.9	14.0	46.1	46.6	57.6	14.0	46.2	47.1
LoSA-S (Mercea et al., 2024)	IN-1k	29.8	10.7	45.7	46.7	54.9	10.7	45.8	46.6
META-S_(Ours)	IN-1k	29.4	5.9	46.9	49.5	54.7	5.9	47.2	48.0
Twins-SVT-L (Chu et al., 2021)	IN-1k	103.7	NA	46.7	45.5	133.0	NA	48.8	50.2
ViT-B (Li et al., 2021)	IN-1k	98.0	NA	46.4	47.6	127.3	NA	46.1	47.1
ViT-Adapter-B (Chen et al., 2022b)	IN-1k	104.6	14.0	47.9	48.9	133.9	14.0	48.8	49.7
LoSA-B (Mercea et al., 2024)	IN-1k	103.5	10.7	48.3	49.2	131.2	10.7	47.3	48.5
META-B_(Ours)	IN-1k	100.4	5.9	48.7	49.7	129.1	5.9	49.4	50.5
Swin-L [‡] (Liu et al., 2021)	IN-22k	234.0	NA	–	–	234.0	NA	52.1	53.5
ViT-Adapter-B [‡] (Chen et al., 2022b)	IN-22k	104.6	14.0	50.7	51.9	133.9	14.0	51.9	52.5
ViT-Adapter-L [‡] (Chen et al., 2022b)	IN-22k	332.0	14.0	52.9	53.7	363.8	14.0	53.4	54.4
LoSA-L [‡] (Mercea et al., 2024)	IN-22k	310.5	10.7	52.3	54.0	338.5	10.7	53.0	54.5
META-L[‡]_(Ours)	IN-22k	307.7	5.9	53.7	54.5	336.3	5.9	54.0	55.2
ViT-Adapter-L* (Chen et al., 2022b)	MM	332.0	14.0	54.2	54.7	363.8	14.0	55.0	55.4
LoSA-L* (Mercea et al., 2024)	MM	310.1	10.7	53.3	54.5	341.0	10.7	55.1	55.5
META-L*_(Ours)	MM	307.7	5.9	54.7	55.2	336.3	5.9	55.6	55.9

Table 3: Result comparisons with SOTA methods on the *val* set of ADE20K. “–” denotes there is no such a result in its paper. “IN” and “MM” denotes ImageNet and Multi-Modal, respectively.

ISeg and ODet results on the <i>val</i> set of MS-COCO (Caesar et al., 2018)										
ViT-B (Li et al., 2021)	Attn Branch.	FFN Branch.	Conv Branch.	Cascade	AP ^m	AP ^b	#P	FLOPs	MC	FPS
✓					41.3	45.8	113.6	719	NA	11.5
✓	✓				32.1	33.6	113.9	719	7.5	11.3
✓	✓	✓			43.4	46.5	114.4	719	7.5	11.3
✓	✓	✓			30.8	31.2	114.0	719	0.4	11.4
✓	✓	✓	✓		44.1	48.1	115.3	719	7.5	10.2
✓	✓	✓	✓	✓	43.6	49.3	114.4	720	8.1	11.0
✓	✓	✓	✓	✓	44.3	51.2	115.3	720	8.1	11.1
SSeg results on the <i>val</i> set of ADE20K (Zhou et al., 2017)										
UperNet (Xiao et al., 2018)	Attn Branch.	FFN Branch.	Conv Branch.	Cascade	mIoU	#P	FLOPs	MC	FPS	
✓					46.1	127.3	1,841	NA	25.4	
✓	✓				33.7	128.0	1,843	5.1	25.0	
✓	✓	✓			46.8	128.5	1,846	5.1	24.9	
✓	✓	✓			31.1	128.1	1,841	0.3	25.0	
✓	✓	✓	✓		47.9	129.0	1,847	5.1	23.5	
✓	✓	✓	✓	✓	48.0	128.6	1,846	5.9	25.0	
✓	✓	✓	✓	✓	49.4	129.1	1,847	5.9	24.9	

Table 4: Effectiveness of each component of META. “NA” denotes not applicable.

41.3% to 32.1% and from 45.8% to 33.6%). This indicates that using attention alone as the feature interaction method in the adapter is not enough. Then, on this basis, when we use both the Attn branch and FFN branch as adapter components (where the layer normalization is used as a shared manner), the model’s accuracy is significantly improved, surpassing the baseline model by 2.1% AP^m/0.7% AP^b and achieving 43.4% AP^m/46.5% AP^b. At the same time, the model only has a small increase in parameters and no increase in FLOPs. The same conclusion can be drawn from the SSeg task. *Furthermore, the independent utilization of the FFN branch as the adapter component does not yield an improvement in accuracy. Instead, it significantly detracts from the model’s accuracy across all three tasks evaluated.* After that, continuing to add the Conv branch or using the

cascaded mechanism can bring sustained performance improvement, *e.g.*, 0.7% and 0.2% AP^m, and 1.6% and 2.8% AP^b, respectively. Finally, when using all components in the adapter, the model for ISeg and ODet achieves the best performance by 44.3% AP^m and 51.2% AP^b with 115.3M parameters, 720G FLOPs, 8.1GB MC, and 11.1 FPS. The model for SSeg achieves the best accuracy by 49.4 mIoU with 129.1M parameters, 1847G FLOPs, 5.9GB MC, and 24.9 FPS. In addition, results in the ablation analysis reveal that the increase in the model’s FLOPs and MC is mainly attributed to the utilization of the “cascade” mechanism. Despite this, this mechanism can lead to significant improvements in both accuracy and speed.

5 CONCLUSION

We proposed a simple and fast META that aims at improving the ViT model’s memory efficiency and reduce memory time consumption by minimizing layer normalization and frequent reshaping operations. The main contribution of this work was the proposal of the MEA block that shares the layer normalization between the self-attention and feed-forward network layers, which exist in a parallel manner. Within the proposed block, the cross-shaped self-attention was employed to reduce the requirements for frequent reshaping operations. Moreover, a lightweight local convolutional branch is introduced into META to enrich local inductive biases. Experimental results on object detection, instance segmentation, and semantic segmentation tasks demonstrated that META can achieve a new state-of-the-art accuracy-cost trade-off and at a faster inference speed. In addition to the experimental validation, we also theoretical proved that META exhibits superior generalization capability and stronger adaptability compared to current ViT adapters. In the future, we will explore the effectiveness of META on more ViT architectures, such as designing memory-efficient ViT models for a wider range of computer vision tasks. Besides, reducing the model’s memory footprint is identified as a promising research direction to be explored for LLMs.

ACKNOWLEDGMENT

The authors would like to thank all anonymous reviewers for their positive comments and constructive suggestions. This work was partially supported by the Hong Kong SAR RGC General Research Fund under Grant 16208823 and ACCESS - AI Chip Center for Emerging Smart Systems, sponsored by InnoHK funding, Hong Kong SAR.

REFERENCES

- Michael Arbel, Anna Korba, Adil Salim, and Arthur Gretton. Maximum mean discrepancy gradient flow. In *NeurIPS*, 2019. 16, 17
- Holger Caesar, Jasper Uijlings, and Vittorio Ferrari. Coco-stuff: Thing and stuff classes in context. In *CVPR*, pp. 1209–1218, 2018. 6, 8, 9, 17, 18, 20, 21
- Zhaowei Cai and Nuno Vasconcelos. Cascade r-cnn: High quality object detection and instance segmentation. *IEEE transactions on pattern analysis and machine intelligence*, 43(5):1483–1498, 2019. 6, 7, 8
- Hanting Chen, Yunhe Wang, Tianyu Guo, Chang Xu, Yiping Deng, Zhenhua Liu, Siwei Ma, Chung-jing Xu, Chao Xu, and Wen Gao. Pre-trained image processing transformer. In *CVPR*, pp. 12299–12310, 2021. 1
- Kai Chen, Jiaqi Wang, Jiangmiao Pang, Yuhang Cao, Yu Xiong, Xiaoxiao Li, Shuyang Sun, Wansen Feng, Ziwei Liu, Jiarui Xu, et al. Mmdetection: Open mmlab detection toolbox and benchmark. *arXiv*, 2019. 18
- Shoufa Chen, Chongjian Ge, Zhan Tong, Jiangliu Wang, Yibing Song, Jue Wang, and Ping Luo. Adaptformer: Adapting vision transformers for scalable visual recognition. In *NeurIPS*, pp. 16664–16678, 2022a. 5, 6, 7
- Zhe Chen, Yuchen Duan, Wenhai Wang, Junjun He, Tong Lu, Jifeng Dai, and Yu Qiao. Vision transformer adapter for dense predictions. In *ICLR*, 2022b. 1, 2, 3, 6, 7, 8, 9, 16, 17, 18, 19

- Xiuyuan Cheng and Yao Xie. Neural tangent kernel maximum mean discrepancy. In *NeurIPS*, pp. 6658–6670, 2021. 16, 17
- Xiangxiang Chu, Zhi Tian, Yuqing Wang, Bo Zhang, Haibing Ren, Xiaolin Wei, Huaxia Xia, and Chunhua Shen. Twins: Revisiting the design of spatial attention in vision transformers. In *NeurIPS*, pp. 9355–9366, 2021. 9
- MMSegmentation Contributors. MMSegmentation: Openmmlab semantic segmentation toolbox and benchmark. <https://github.com/open-mmlab/mms Segmentation>, 2020. 18
- Tri Dao, Dan Fu, Stefano Ermon, Atri Rudra, and Christopher Ré. Flashattention: Fast and memory-efficient exact attention with io-awareness. In *NeurIPS*, pp. 16344–16359, 2022. 2
- Jia Deng, Wei Dong, Richard Socher, Li-Jia Li, Kai Li, and Li Fei-Fei. Imagenet: A large-scale hierarchical image database. In *CVPR*, pp. 248–255, 2009. 6, 18
- Peiyang Dong, Lei Lu, Chao Wu, Cheng Lyu, Geng Yuan, Hao Tang, and Yanzhi Wang. Packqvit: Faster sub-8-bit vision transformers via full and packed quantization on the mobile. In *NeurIPS*, 2024a. 2
- Wei Dong, Dawei Yan, Zhijun Lin, and Peng Wang. Efficient adaptation of large vision transformer via adapter re-composing. In *NeurIPS*, 2024b. 5
- Xiaoyi Dong, Jianmin Bao, Dongdong Chen, Weiming Zhang, Nenghai Yu, Lu Yuan, Dong Chen, and Baining Guo. Cswin transformer: A general vision transformer backbone with cross-shaped windows. In *CVPR*, pp. 12124–12134, 2022. 4, 19
- Alexey Dosovitskiy, Lucas Beyer, Alexander Kolesnikov, Dirk Weissenborn, Xiaohua Zhai, Thomas Unterthiner, Mostafa Dehghani, Matthias Minderer, Georg Heigold, Sylvain Gelly, et al. An image is worth 16x16 words: Transformers for image recognition at scale. In *ICLR*, 2020. 1, 2, 3
- Yifan Du, Zikang Liu, Junyi Li, and Wayne Xin Zhao. A survey of vision-language pre-trained models. *arXiv*, 2022. 1
- Quentin Fournier, Gaétan Marceau Caron, and Daniel Aloise. A practical survey on faster and lighter transformers. *ACM Computing Surveys*, 55(14s):1–40, 2023. 2
- Marylou Gabrié, Andre Manoel, Clément Luneau, Nicolas Macris, Florent Krzakala, Lenka Zdeborová, et al. Entropy and mutual information in models of deep neural networks. In *NeurIPS*, 2018. 16
- Peng Gao, Shijie Geng, Renrui Zhang, Teli Ma, Rongyao Fang, Yongfeng Zhang, Hongsheng Li, and Yu Qiao. Clip-adapter: Better vision-language models with feature adapters. *International Journal of Computer Vision*, pp. 1–15, 2023. 1
- Jiaqi Gu, Hanqing Zhu, Chenghao Feng, Mingjie Liu, Zixuan Jiang, Ray T Chen, and David Z Pan. Towards memory-efficient neural networks via multi-level in situ generation. In *ICCV*, pp. 5229–5238, 2021. 2
- Jiaqi Gu, Hyoukjun Kwon, Dilin Wang, Wei Ye, Meng Li, Yu-Hsin Chen, Liangzhen Lai, Vikas Chandra, and David Z Pan. Multi-scale high-resolution vision transformer for semantic segmentation. In *CVPR*, pp. 12094–12103, 2022. 3
- Meng-Hao Guo, Tian-Xing Xu, Jiang-Jiang Liu, Zheng-Ning Liu, Peng-Tao Jiang, Tai-Jiang Mu, Song-Hai Zhang, Ralph R Martin, Ming-Ming Cheng, and Shi-Min Hu. Attention mechanisms in computer vision: A survey. *Computational Visual Media*, 8(3):331–368, 2022. 3
- Kai Han, Yunhe Wang, Hanting Chen, Xinghao Chen, Jianyuan Guo, Zhenhua Liu, Yehui Tang, An Xiao, Chunjing Xu, Yixing Xu, et al. A survey on vision transformer. *IEEE transactions on pattern analysis and machine intelligence*, 45(1):87–110, 2022. 1, 2
- Ali Hatamizadeh, Vishwesh Nath, Yucheng Tang, Dong Yang, Holger R Roth, and Daguang Xu. Swin unetr: Swin transformers for semantic segmentation of brain tumors in mri images. In *MICCAI Workshop*, pp. 272–284, 2021. 3

- Bobby He and Thomas Hofmann. Simplifying transformer blocks. In *ICLR*, 2024. 2, 3, 4, 5, 19
- Kaiming He, Georgia Gkioxari, Piotr Dollár, and Ross Girshick. Mask r-cnn. In *ICCV*, pp. 2961–2969, 2017. 6, 7, 8, 18
- Kaiming He, Xinlei Chen, Saining Xie, Yanghao Li, Piotr Dollár, and Ross Girshick. Masked autoencoders are scalable vision learners. In *CVPR*, pp. 16000–16009, 2022. 1, 3
- Neil Houlsby, Andrei Giurgiu, Stanislaw Jastrzebski, Bruna Morrone, Quentin De Laroussilhe, Andrea Gesmundo, Mona Attariyan, and Sylvain Gelly. Parameter-efficient transfer learning for nlp. In *ICML*, pp. 2790–2799, 2019. 1, 3
- Edward J Hu, Yelong Shen, Phillip Wallis, Zeyuan Allen-Zhu, Yanzhi Li, Shean Wang, Lu Wang, and Weizhu Chen. LoRA: Low-rank adaptation of large language models. In *ICLR*, 2022. 1, 3, 16, 17
- Jie Hu, Liujuan Cao, Yao Lu, ShengChuan Zhang, Yan Wang, Ke Li, Feiyue Huang, Ling Shao, and Rongrong Ji. Istr: End-to-end instance segmentation with transformers. *arXiv*, 2021. 3
- Andrei Ivanov, Nikoli Dryden, Tal Ben-Nun, Shigang Li, and Torsten Hoeffler. Data movement is all you need: A case study on optimizing transformers. In *MLSys*, pp. 711–732, 2021. 2
- Menglin Jia, Luming Tang, Bor-Chun Chen, Claire Cardie, Serge Belongie, Bharath Hariharan, and Ser-Nam Lim. Visual prompt tuning. In *ECCV*, pp. 709–727, 2022. 3
- Shibo Jie and Zhi-Hong Deng. Convolutional bypasses are better vision transformer adapters. *arXiv*, 2022. 1, 3, 6, 7
- Shibo Jie and Zhi-Hong Deng. Fact: Factor-tuning for lightweight adaptation on vision transformer. In *AAAI*, pp. 1060–1068, 2023. 1, 2, 3, 6, 7, 16, 17
- Salman Khan, Muzammal Naseer, Munawar Hayat, Syed Waqas Zamir, Fahad Shahbaz Khan, and Mubarak Shah. Transformers in vision: A survey. *ACM computing surveys*, 54(10s):1–41, 2022. 1, 2
- Alexander Kirillov, Ross Girshick, Kaiming He, and Piotr Dollár. Panoptic feature pyramid networks. In *CVPR*, pp. 6399–6408, 2019. 7
- Alexander Kirillov, Eric Mintun, Nikhila Ravi, Hanzi Mao, Chloe Rolland, Laura Gustafson, Tete Xiao, Spencer Whitehead, Alexander C. Berg, Wan-Yen Lo, Piotr Dollar, and Ross Girshick. Segment anything. In *ICCV*, pp. 4015–4026, 2023. 1, 2
- Jiashi Li, Xin Xia, Wei Li, Huixia Li, Xing Wang, Xuefeng Xiao, Rui Wang, Min Zheng, and Xin Pan. Next-vit: Next generation vision transformer for efficient deployment in realistic industrial scenarios. *arXiv*, 2022a. 3, 5
- Xiang Li, Wenhai Wang, Lijun Wu, Shuo Chen, Xiaolin Hu, Jun Li, Jinhui Tang, and Jian Yang. Generalized focal loss: Learning qualified and distributed bounding boxes for dense object detection. In *NeurIPS*, pp. 21002–21012, 2020. 6, 8
- Yanghao Li, Saining Xie, Xinlei Chen, Piotr Dollar, Kaiming He, and Ross Girshick. Benchmarking detection transfer learning with vision transformers. *arXiv*, 2021. 3, 6, 7, 8, 9
- Yanghao Li, Hanzi Mao, Ross Girshick, and Kaiming He. Exploring plain vision transformer backbones for object detection. In *ECCV*, pp. 280–296. Springer, 2022b. 2, 3, 6, 7, 8, 18, 19
- Tsung-Yi Lin, Michael Maire, Serge Belongie, James Hays, Pietro Perona, Deva Ramanan, Piotr Dollár, and C Lawrence Zitnick. Microsoft coco: Common objects in context. In *ECCV*, pp. 740–755, 2014. 2
- Xinyu Liu, Houwen Peng, Ningxin Zheng, Yuqing Yang, Han Hu, and Yixuan Yuan. Efficientvit: Memory efficient vision transformer with cascaded group attention. In *CVPR*, pp. 14420–14430, 2023. 2, 3, 17

- Yifei Liu, Mathias Gehrig, Nico Messikommer, Marco Cannici, and Davide Scaramuzza. Revisiting token pruning for object detection and instance segmentation. In *WACV*, pp. 2658–2668, 2024. [2](#)
- Ze Liu, Yutong Lin, Yue Cao, Han Hu, Yixuan Wei, Zheng Zhang, Stephen Lin, and Baining Guo. Swin transformer: Hierarchical vision transformer using shifted windows. In *ICCV*, pp. 10012–10022, 2021. [1](#), [2](#), [3](#), [7](#), [8](#), [9](#), [18](#), [19](#)
- Zhuang Liu, Hanzi Mao, Chao-Yuan Wu, Christoph Feichtenhofer, Trevor Darrell, and Saining Xie. A convnet for the 2020s. In *CVPR*, pp. 11976–11986, 2022. [18](#)
- Ilya Loshchilov and Frank Hutter. Decoupled weight decay regularization. *arXiv*, 2017. [18](#)
- Anwei Luo, Rizhao Cai, Chenqi Kong, Xiangui Kang, Jiwu Huang, and Alex C Kot. Forgery-aware adaptive vision transformer for face forgery detection. *arXiv*, 2023. [1](#), [3](#), [16](#), [17](#), [18](#)
- Jun Ma, Yuting He, Feifei Li, Lin Han, Chenyu You, and Bo Wang. Segment anything in medical images. *Nature Communications*, 15(1):654, 2024. [1](#), [16](#), [17](#)
- Imad Eddine Marouf, Enzo Tartaglione, and Stéphane Lathuilière. Mini but mighty: Finetuning vits with mini adapters. In *WACV*, pp. 1732–1741, 2024. [2](#), [5](#), [6](#), [17](#), [19](#)
- Otniel-Bogdan Mercea, Alexey Gritsenko, Cordelia Schmid, and Anurag Arnab. Time-memory-and parameter-efficient visual adaptation. In *CVPR*, pp. 5536–5545, 2024. [3](#), [6](#), [7](#), [8](#), [9](#), [17](#), [18](#)
- Zizheng Pan, Jianfei Cai, and Bohan Zhuang. Fast vision transformers with hilo attention. In *NeurIPS*, pp. 14541–14554, 2022. [2](#)
- Liam Paninski. Estimation of entropy and mutual information. *Neural Computation*, 15(6):1191–1253, 2003. [16](#)
- Zhiliang Peng, Wei Huang, Shanzhi Gu, Lingxi Xie, Yaowei Wang, Jianbin Jiao, and Qixiang Ye. Conformer: Local features coupling global representations for visual recognition. In *ICCV*, pp. 367–376, 2021. [3](#), [5](#), [16](#)
- Alec Radford, Jong Wook Kim, Chris Hallacy, Aditya Ramesh, Gabriel Goh, Sandhini Agarwal, Girish Sastry, Amanda Askell, Pamela Mishkin, Jack Clark, et al. Learning transferable visual models from natural language supervision. In *ICML*, pp. 8748–8763, 2021. [1](#)
- René Ranftl, Alexey Bochkovskiy, and Vladlen Koltun. Vision transformers for dense prediction. In *ICCV*, pp. 12179–12188, 2021. [3](#)
- Andrew M Saxe, James L McClelland, and Surya Ganguli. Exact solutions to the nonlinear dynamics of learning in deep linear neural networks. *arXiv*, 2013. [5](#)
- Rui Shao, Tianxing Wu, Liqiang Nie, and Ziwei Liu. Deepfake-adapter: Dual-level adapter for deepfake detection. *International Journal of Computer Vision*, 2024. [1](#), [3](#), [16](#), [17](#)
- Wei Shen, Zelin Peng, Xuehui Wang, Huayu Wang, Jiazhong Cen, Dongsheng Jiang, Lingxi Xie, Xiaokang Yang, and Q Tian. A survey on label-efficient deep image segmentation: Bridging the gap between weak supervision and dense prediction. *IEEE Transactions on Pattern Analysis and Machine Intelligence*, 2023. [3](#)
- Yulong Shi, Mingwei Sun, Yongshuai Wang, Rui Wang, Hui Sun, and Zengqiang Chen. Evit: An eagle vision transformer with bi-fovea self-attention. *arXiv*, 2023. [2](#)
- Andreas Steiner, Alexander Kolesnikov, Xiaohua Zhai, Ross Wightman, Jakob Uszkoreit, and Lucas Beyer. How to train your vit? data, augmentation, and regularization in vision transformers. *Transactions on Machine Learning Research (TMLR)*, 2021. [6](#), [7](#), [18](#), [21](#)
- Asa Cooper Stickland and Iain Murray. Bert and pals: Projected attention layers for efficient adaptation in multi-task learning. In *ICML*, pp. 5986–5995, 2019. [3](#)
- Robin Strudel, Ricardo Garcia, Ivan Laptev, and Cordelia Schmid. Segmenter: Transformer for semantic segmentation. In *ICCV*, pp. 7262–7272, 2021. [3](#)

- Yi-Lin Sung, Jaemin Cho, and Mohit Bansal. Vi-adapter: Parameter-efficient transfer learning for vision-and-language tasks. In *CVPR*, pp. 5227–5237, 2022. 19
- Ilya O Tolstikhin, Neil Houlsby, Alexander Kolesnikov, Lucas Beyer, Xiaohua Zhai, Thomas Unterthiner, Jessica Yung, Andreas Steiner, Daniel Keysers, Jakob Uszkoreit, et al. Mlp-mixer: An all-mlp architecture for vision. In *NeurIPS*, pp. 24261–24272, 2021. 5
- Hugo Touvron, Matthieu Cord, Matthijs Douze, Francisco Massa, Alexandre Sablayrolles, and Hervé Jégou. Training data-efficient image transformers & distillation through attention. In *ICML*, pp. 10347–10357, 2021. 1, 2
- Zhengzhong Tu, Hossein Talebi, Han Zhang, Feng Yang, Peyman Milanfar, Alan Bovik, and Yinxiao Li. Maxvit: Multi-axis vision transformer. In *ECCV*, pp. 459–479, 2022. 4
- Simon Vandenhende, Stamatios Georgoulis, Wouter Van Gansbeke, Marc Proesmans, Dengxin Dai, and Luc Van Gool. Multi-task learning for dense prediction tasks: A survey. *IEEE Transactions on Pattern Analysis and Machine Intelligence*, 44(7):3614–3633, 2021. 3
- Ashish Vaswani, Noam Shazeer, Niki Parmar, Jakob Uszkoreit, Llion Jones, Aidan N Gomez, Łukasz Kaiser, and Illia Polosukhin. Attention is all you need. In *NeurIPS*, 2017. 4, 5, 19
- Anand Venkat, Tharindu Rusira, Raj Barik, Mary Hall, and Leonard Truong. Swirl: High-performance many-core cpu code generation for deep neural networks. *The International Journal of High Performance Computing Applications*, 33(6):1275–1289, 2019. 2
- Ben Wang and Aran Komatsuzaki. Gpt-j-6b: A 6 billion parameter autoregressive language model, 2021. 4
- Wei Wang, Haojie Li, Zhengming Ding, Feiping Nie, Junyang Chen, Xiao Dong, and Zhihui Wang. Rethinking maximum mean discrepancy for visual domain adaptation. *IEEE Transactions on Neural Networks and Learning Systems*, 34(1):264–277, 2021a. 16, 17
- Wenhai Wang, Enze Xie, Xiang Li, Deng-Ping Fan, Kaitao Song, Ding Liang, Tong Lu, Ping Luo, and Ling Shao. Pyramid vision transformer: A versatile backbone for dense prediction without convolutions. In *ICCV*, pp. 568–578, 2021b. 2, 3, 7, 9, 18
- Haiping Wu, Bin Xiao, Noel Codella, Mengchen Liu, Xiyang Dai, Lu Yuan, and Lei Zhang. Cvt: Introducing convolutions to vision transformers. In *ICCV*, pp. 22–31, 2021. 3, 5, 16
- Sitong Wu, Tianyi Wu, Haoru Tan, and Guodong Guo. Pale transformer: A general vision transformer backbone with pale-shaped attention. In *AAAI*, pp. 2731–2739, 2022. 19
- Zhuofan Xia, Xuran Pan, Shiji Song, Li Erran Li, and Gao Huang. Vision transformer with deformable attention. In *CVPR*, pp. 4794–4803, 2022. 19
- Tete Xiao, Yingcheng Liu, Bolei Zhou, Yuning Jiang, and Jian Sun. Unified perceptual parsing for scene understanding. In *ECCV*, pp. 418–434, 2018. 7, 8, 9
- Enze Xie, Wenhai Wang, Zhiding Yu, Anima Anandkumar, Jose M Alvarez, and Ping Luo. Segformer: Simple and efficient design for semantic segmentation with transformers. In *NeurIPS*, pp. 12077–12090, 2021. 2
- Yuwen Xiong, Zhiqi Li, Yuntao Chen, Feng Wang, Xizhou Zhu, Jiapeng Luo, Wenhai Wang, Tong Lu, Hongsheng Li, Yu Qiao, et al. Efficient deformable convnets: Rethinking dynamic and sparse operator for vision applications. *arXiv*, 2024. 6, 18
- Bowen Zhang, Zhi Tian, Quan Tang, Xiangxiang Chu, Xiaolin Wei, Chunhua Shen, et al. Segvit: Semantic segmentation with plain vision transformers. In *NeurIPS*, pp. 4971–4982, 2022a. 3
- Dong Zhang, Jinhui Tang, and Kwang-Ting Cheng. Graph reasoning transformer for image parsing. In *ACM MM*, pp. 2380–2389, 2022b. 16, 17
- Dong Zhang, Chengting Zuo, Qianhao Wu, Liyong Fu, and Xinguang Xiang. Unabridged adjacent modulation for clothing parsing. *Pattern Recognition*, 127:108594, 2022c. 1

- Dong Zhang, Yi Lin, Jinhui Tang, and Kwang-Ting Cheng. Cae-great: Convolutional-auxiliary efficient graph reasoning transformer for dense image predictions. *International Journal of Computer Vision*, pp. 1–19, 2023. 1, 3, 5, 16, 17, 18
- Dong Zhang, Pingcheng Dong, Xinting Hu, Long Chen, and Kwang-Ting Cheng. Boundary and relation distillation for semantic segmentation. *arXiv*, 2024. 1, 3
- Shifeng Zhang, Cheng Chi, Yongqiang Yao, Zhen Lei, and Stan Z Li. Bridging the gap between anchor-based and anchor-free detection via adaptive training sample selection. In *CVPR*, pp. 9759–9768, 2020. 6, 8
- Bolei Zhou, Hang Zhao, Xavier Puig, Sanja Fidler, Adela Barriuso, and Antonio Torralba. Scene parsing through ade20k dataset. In *CVPR*, pp. 633–641, 2017. 2, 6, 8, 9, 17, 21
- Xizhou Zhu, Jinguo Zhu, Hao Li, Xiaoshi Wu, Hongsheng Li, Xiaohua Wang, and Jifeng Dai. Uni-perceiver: Pre-training unified architecture for generic perception for zero-shot and few-shot tasks. In *CVPR*, pp. 16804–16815, 2022. 18, 21

SUPPLEMENTARY MATERIAL

In this supplementary material, we will provide a theoretical analysis to the proposed memory efficient Transformer adapter (META) in Section 6, provide a detailed description of the experimental datasets in Section 7, provide a detailed description of the experimental settings in Section 8, provide more result comparisons under different pre-trained weights in Section 9, provide more ablation study results in Section 10, show class activation map comparisons of instance segmentation before and after adding the Conv branch in Section 11, qualitative visualizations of instance segmentation and semantic segmentation results in Section 12, as well as the pseudo-code for when the stripe size is set to 2 in Section 13.

6 THEORETICAL ANALYSIS OF META

This supplementary is for Section 3 of the main paper. In this section, we will prove that META exhibits superior generalization capability and stronger adaptability compared to existing ViT adapters. To achieve this goal, we will prove that the proposed memory efficient adapter (MEA) block possesses larger information entropy (IE) than the existing attention-based ViT adapters (Hu et al., 2022; Jie & Deng, 2023; Chen et al., 2022b; Ma et al., 2024; Luo et al., 2023; Shao et al., 2024), which provides evidence that the MEA block has more comprehensive feature representations. Then, based on the maximum mean discrepancy (MMD) theory (Cheng & Xie, 2021; Arbel et al., 2019; Wang et al., 2021a), larger IE in the ViT adapter framework leads to superior generalization capability and stronger adaptability. The detailed theoretical analysis process is as follows:

Lemma 6.1. *In any case of mutual information, the MEA block will gain larger information entropy after fusing \mathbf{X}_{vit} and \mathbf{X}_{con} .*

Proof. As introduced in Section 3.2 of the main paper, the proposed MEA block can be viewed as an operation that integrates the ViT features (*i.e.*, the Attn branch and the FFN branch) and the convolution features (*i.e.*, the Conv branch). Therefore, we begin by formalizing the obtained features into the following two basic elements: the ViT features and the convolution features. To formalize the learning setting, we express the ViT features as \mathbf{X}_{vit} and the convolution features as \mathbf{X}_{con} . It is evident that if \mathbf{X}_{vit} and \mathbf{X}_{con} are extracted from the same image, then \mathbf{X}_{vit} and \mathbf{X}_{con} are not independently distributed, and there exists some mutual information between them (Zhang et al., 2022b; Wu et al., 2021; Zhang et al., 2023; Peng et al., 2021). Therefore, the IE of the fused feature of \mathbf{X}_{vit} and \mathbf{X}_{con} within the MEA block can be expressed as:

$$H(\mathbf{X}_{vit}, \mathbf{X}_{con}) = H(\mathbf{X}_{vit}) + H(\mathbf{X}_{con}) - I(\mathbf{X}_{vit}; \mathbf{X}_{con}), \quad (6)$$

where $H(\cdot)$ is utilized to calculate the IE of the given variate, which can be formulated as:

$$\begin{aligned} H(\mathbf{X}_{vit}) &= - \sum P(\mathbf{x}_{vit}) \log(P(\mathbf{x}_{vit})), \\ H(\mathbf{X}_{con}) &= - \sum P(\mathbf{x}_{con}) \log(P(\mathbf{x}_{con})), \end{aligned} \quad (7)$$

where $P(\mathbf{x}_{vit})$ represents the probability of \mathbf{X}_{vit} taking on the value of \mathbf{x}_{vit} . The similar definition of $P(\mathbf{x}_{con})$. $I(\cdot; \cdot)$ in Eq. equation 6 is used to compute the mutual information between \mathbf{X}_{vit} and \mathbf{X}_{con} , which can be expressed as:

$$I(\mathbf{X}_{vit}; \mathbf{X}_{con}) = \sum \sum P(\mathbf{X}_{vit}, \mathbf{X}_{con}) \log(P(\mathbf{X}_{vit}, \mathbf{X}_{con}) / (P(\mathbf{X}_{vit})P(\mathbf{X}_{con}))), \quad (8)$$

where $P(\mathbf{X}_{vit}, \mathbf{X}_{con})$ is their joint probability distribution. Since $I(\mathbf{X}_{vit}; \mathbf{X}_{con})$ is always non-negative, $H(\mathbf{X}_{vit}, \mathbf{X}_{con})$ may still be greater than $H(\mathbf{X}_{vit})$ or $H(\mathbf{X}_{con})$ (Paninski, 2003; Gabri el et al., 2018). This suggests that the IE of the features extracted by MEA is always greater than the feature representation extracted by either of them separately.

Specifically, if $I(\mathbf{X}_{vit}; \mathbf{X}_{con})$ is small, the IE gain after fusion may still be significant, which is beneficial for improving the generalization capability and adaptability of the block. However, when $I(\mathbf{X}_{vit}; \mathbf{X}_{con})$ is large, the IE gain after fusion may be reduced. This means that $I(\mathbf{X}_{vit}; \mathbf{X}_{con})$ may affect the IE improvement of the fused model. Next, we will discuss the impact of \mathbf{X}_{vit} and \mathbf{X}_{con} on improving the IE of the adapter based on the size of $I(\mathbf{X}_{vit}; \mathbf{X}_{con})$, which can be divided into the following three cases:

- Small $I(\mathbf{X}_{vit}; \mathbf{X}_{con})$. This is an ideal state. When the dependency between \mathbf{X}_{vit} and \mathbf{X}_{con} is small, it indicates that $I(\mathbf{X}_{vit}; \mathbf{X}_{con})$ is small, that is, \mathbf{X}_{vit} and \mathbf{X}_{con} respectively represent different information of the image. In this case, fusing \mathbf{X}_{vit} and \mathbf{X}_{con} can bring a significant increase in IE, which is beneficial to improving the adapter’s generalization capability and adaptability.
- Medium $I(\mathbf{X}_{vit}; \mathbf{X}_{con})$. When $I(\mathbf{X}_{vit}; \mathbf{X}_{con})$ is between small and large, it indicates that there is a certain degree of correlation between them. In this case, fusing \mathbf{X}_{vit} and \mathbf{X}_{con} may still bring some IE gain. The specific improvement effect depends on the degree of correlation between \mathbf{X}_{vit} and \mathbf{X}_{con} and their complementarity in image representations. Fortunately (Zhang et al., 2022b; 2023; Marouf et al., 2024; Liu et al., 2023), a large amount of work has validated that ViT and convolutional layers can extract distinctive information from images. Therefore, in this case, fusing \mathbf{X}_{vit} and \mathbf{X}_{con} can still bring IE gains.
- Large $I(\mathbf{X}_{vit}; \mathbf{X}_{con})$. When $I(\mathbf{X}_{vit}; \mathbf{X}_{con})$ between \mathbf{X}_{vit} and \mathbf{X}_{con} is large, it indicates that there is a high correlation between them, *i.e.*, global ViT and local convolution features may represent similar or overlapping information of the image. In this case, the IE gain brought by fusing \mathbf{X}_{vit} and \mathbf{X}_{con} may decrease because there is a lot of information overlap between them. However, in our case, the probability of such a scenario occurring is almost non-existent, fusing \mathbf{X}_{vit} and \mathbf{X}_{con} may still improve the performance of the model to some extent, because they may capture the detailed information of the image to varying degrees.

Based on the aforementioned theoretical analysis, we can conclude that the proposed MEA block has a larger IE than existing ViT adapters (which are primarily based on the attention mechanism) under any scenario. This provides evidence that the MEA block has more comprehensive feature representations. \square

As the MEA block includes a parallel convolutional branch, it can better capture local inductive biases compared to the traditional ViT adapter, which mainly uses self-attention (Hu et al., 2022; Jie & Deng, 2023; Chen et al., 2022b; Ma et al., 2024; Luo et al., 2023; Shao et al., 2024; Mercea et al., 2024). Therefore, the MEA block’s feature space should be more capable of distinguishing different samples, resulting in a larger MMD value. Our MEA block’s feature space is obtained by combining the attention branch, the feed-forward network branch, and the local convolutional branch, enabling it to capture both local and global inductive biases of the given image. In contrast, the traditional ViT adapter’s feature space is mainly obtained through self-attention and may not be able to capture local features well. Therefore, according to the MMD theory (Cheng & Xie, 2021; Arbel et al., 2019; Wang et al., 2021a), we can conclude that if the MEA block’s feature space is more discriminative than the traditional ViT adapter’s feature space, then the MEA block’s feature space is more suitable for adapter feature space and can better improve the model’s generalization capability and adaptability.

7 INTRODUCTION OF THE EXPERIMENTAL DATASETS

This supplementary is for Section 4.1 of the main paper. In our paper, two representative datasets are used to evaluate the effectiveness and efficiency of our method, including MS-COCO (Caesar et al., 2018) for ODet and ISeg, and ADE20K (Zhou et al., 2017) for SSeg. Below are the details of the used datasets:

- MS-COCO (Caesar et al., 2018) is a representative yet challenging dataset for common scene IS and object detection, which consists of 118k, 5k and 20k images for the *training* set, the *val* set and the *test* set, respectively. In our experiments, the model is trained on the *training* set and evaluated on the *val* set.
- ADE20K (Zhou et al., 2017) is a scene parsing dataset with 20k images and 150 object categories. Each image has pixel-level annotations for SS of objects and regions within the scene. The dataset is divided into 20k, 2k, and 3k images for *training*, *val* and *test*, respectively. Our model is trained on the *training* set and evaluated on the *val* set.

Methods	Pre-Trained	Params.↓	AP ^m ↑
Swin-B (Liu et al., 2021)	ImageNet-1k (Deng et al., 2009)	107.1	43.3
ViT-Adapter-B (Chen et al., 2022b)	ImageNet-1k (Deng et al., 2009)	120.2	43.6
META-B_(Ours)	ImageNet-1k (Deng et al., 2009)	115.3	44.3 _{+0.7}
Swin-B (Liu et al., 2021)	ImageNet-22k (Steiner et al., 2021)	107.1	44.3
ViT-Adapter-B (Chen et al., 2022b)	ImageNet-22k (Steiner et al., 2021)	120.2	44.6
META-B_(Ours)	ImageNet-22k (Steiner et al., 2021)	115.3	45.2 _{+0.6}
Swin-B (Liu et al., 2021)	Multi-Modal (Zhu et al., 2022)	107.1	–
ViT-Adapter-B (Chen et al., 2022b)	Multi-Modal (Zhu et al., 2022)	120.2	45.3
META-B_(Ours)	Multi-Modal (Zhu et al., 2022)	115.3	45.9 _{+0.6}

Table 5: Result comparisons on Params. (M) and AP (%) under different pre-trained weights with Mask R-CNN (3× +MS schedule) (He et al., 2017) as the baseline model on the *val* set of MSCOCO (Caesar et al., 2018). “–” denotes there is no such a result in its paper.

For data augmentation, random horizontal flip, brightness jittering and random scaling within the range of $[0.5, 2]$ are used in training as in (Chen et al., 2022b; Luo et al., 2023; Zhang et al., 2023; Mercea et al., 2024). By default, the inference results are obtained at a single scale, unless explicitly specified otherwise.

8 INTRODUCTION OF THE EXPERIMENTAL SETTINGS

This supplementary is for Section 4.2 of the main paper. Experiments on object detection and instance segmentation are conducted using the open-source MMDetection framework (Chen et al., 2019). The training batch size is set to 16, and AdamW (Loshchilov & Hutter, 2017) is used as the optimizer with the initial learning rate of 1×10^{-4} and the weight decay of 0.05. The layer-wise learning rate decay is used and set to 0.9, and the drop path rate is set to 0.4. Following (Xiong et al., 2024; Wang et al., 2021b; Chen et al., 2022b; Liu et al., 2022), to ensure a fair result comparison, we choose two training schedules, $1 \times$ (*i.e.*, 12 training epochs) and $3 \times$ (*i.e.*, 36 training epochs). For the $1 \times$ training schedule, images are resized to the shorter side of 800 pixels, with the longer side not exceeding 1,333 pixels. In inference, the shorter side of images is consistently set to 800 pixels by default. For the $3 \times$ training schedule, the multi-scale training strategy is also used as in (Chen et al., 2022b), and the shorter side is resized to 480 to 800 pixels, while the longer side remains capped at 1,333 pixels.

This supplementary is for Section 4.3 of the main paper. Experiments on semantic segmentation are conducted using the MMSegmentation framework (Contributors, 2020). The input images are cropped to a fix size of 512×512 pixels as in (Xiong et al., 2024; Chen et al., 2022b). The training batch size is set to 16, and AdamW (Loshchilov & Hutter, 2017) is used as the optimizer with the initial learning rate of 1×10^{-5} and the weight decay of 0.05. Following (Li et al., 2022b; Liu et al., 2021), the layer-wise learning rate decay is set to 0.9 and the drop path rate is set to 0.4. We report the experimental results on both single scale training and multi-scale training strategies.

9 RESULT COMPARISONS UNDER DIFFERENT WEIGHTS

This supplementary is for Section 4.2 of the main paper. In this section, we present the experimental results of META on object detection and instance segmentation with different pre-trained weights and compare them with other state-of-the-art methods including SwinViT (Liu et al., 2021) and ViT-Adapter (Chen et al., 2022b) as in (Chen et al., 2022b). Mask R-CNN (He et al., 2017) is used as the baseline, and ViT-B (Li et al., 2022b) is used as the backbone. The $3 \times$ training schedule with MS training strategy is used. The obtained experimental results are given in Table 5. From this table, we can observe that our method is applicable to different pre-trained weights (*i.e.*, ImageNet-1k (Deng et al., 2009), ImageNet-22k (Steiner et al., 2021), and Multi-Modal (Zhu et al., 2022)), and achieves more accurate AP with fewer model parameters compared to ViT-Adapter (Chen et al., 2022b), across different pre-trained weights.

Settings	ViT-B	Attn	FFN	Conv	Cascade	AP ^m ↑	FPS ↑	Params. ↓	FLOPs ↓	MC ↓
Baseline model	✓	✗	✗	✗	✗	41.3	11.5	113.6M	719G	NA
Shared normalization	✓	✓	✓	✗	✗	43.4	11.3	114.4M	719G	7.5GB
Non-shared normalization	✓	✓	✓	✗	✗	43.2	10.5	114.4M	737G	8.8GB

Table 6: Ablation study results on shared layer normalization.

Methods	AP ↑	FPS ↑	Params. (M) ↓	FLOPs (G) ↓	Memory (GB) ↓
WindowAtt (Liu et al., 2021)	41.2	11.6	145.0	982	18.5
PaleAttention (Wu et al., 2022)	42.8	14.4	155.2	1,029	16.7
Attention (Vaswani et al., 2017)	43.1	5.2	188.4	1,250	18.3
CSWindow (Dong et al., 2022)	43.1	13.7	144.6	990	12.9
SimplingAtte (He & Hofmann, 2024)	43.3	12.2	126.3	994	17.1
DeformableAtt (Xia et al., 2022)	43.7	13.5	166.0	988	15.2
MiniAdapters (Marouf et al., 2024)	41.9	15.0	131.8	995	12.2
VL-Adapter (Sung et al., 2022)	42.7	14.5	167.2	993	14.0
META-B(Ours)	44.3	17.4	115.3	720	8.1

Table 7: Result comparisons with different adapters.

10 MORE ABLATION STUDY RESULTS

This supplementary is for Section 4.4 of the main paper. In our main paper, we present the experimental results of deploying adapters with Attn branch and FFN branch as components on ViT-B (Li et al., 2022b). It is noteworthy that the layer normalization operation has been shared between the Attn branch and the FFN branch to reduce the memory access costs associated with the normalization operations. In this section, we demonstrate a result comparison between the experimental results of using shared layer normalization operation and those of not using it in the traditional setting (*i.e.*, the non-shared normalization). The obtained experimental results are shown in Table 6. It can be observed that sharing layer normalization does not significantly improve the performance in terms of AP. However, compared to FPS, FLOPs, MC, our approach can achieve satisfactory performance gains.

This supplementary is for Section 4.4 of the main paper. META is proposed as a simple and fast ViT adapter by minimizing inefficient memory access operations. In this section, we compare META with other efficient attention methods and advanced adapter methods (Marouf et al., 2024; Xia et al., 2022; Sung et al., 2022). All methods are used with their default settings and the same settings as the injector and extractor in ViT-adapter (Chen et al., 2022b). Following the same setup as in (Chen et al., 2022b), the attention mechanism is utilized as the ViT-adapter layer. Therefore, during the experimental comparisons, we replace the attention mechanism in the ViT-adapter with alternative attention mechanisms to ensure a fair comparison. The obtained experimental results are given in Table 7. We can observe that compared to these methods, META achieves new state-of-the-art performance in both accuracy and efficiency. We ultimately achieve an AP of 44.3% with 115.3M parameters, 720G FLOPs, 17.4 FPS, and 8.1 GB MC.

11 VISUALIZATIONS UNDER THE CONV BRANCH

This supplementary is for Section 3.2 of the main paper. In this section, to observe if the adapter has learned local inductive biases through the Conv branch, we visualize the model’s class activation maps. The obtained visualizations are given in Figure 3. From this figure, it can be observed that after adding the Conv branch, the model focuses more on the specific object area (*e.g.*, “the dog” and “the person”) rather than the surrounding area that may extend beyond the object itself, as was the case before adding the Conv branch. This indicates that our method effectively learns local inductive biases after incorporating the Conv branch.



Figure 3: Class activation map comparisons of instance segmentation before and after adding the Conv branch. The sample images are from the *training* set of MS-COCO (Caesar et al., 2018).

12 QUALITATIVE VISUALIZATION RESULTS

This supplementary is for Section 4.2 and 4.3 of the main paper. In this section, we show qualitative results on both instance segmentation and semantic segmentation. To demonstrate the superiority of our method, we present visualization results of ablation studies on instance segmentation, as well as comparisons with state-of-the-art methods on both instance segmentation and semantic segmentation. The obtained visualization results are shown in Figure 4. From the results, it can be observed that compared to other methods, our method can achieve more accurate object masks that better fit the actual boundaries of the objects themselves.

as well as the pseudo-code for when the stripe size is set to 2 in Section 13.

13 PSEUDO-CODE FO STRIPE SIZE = 2

In this code snippet, stripe size is set to 2, and relevant features are directly obtained using the gather function instead of reshaping them with `img2windows`. This operation can reduce unnecessary reshaping operations and improves the efficiency of the code.

```
function cross_shaped_window_attention(x, num_heads, window_size):
    # x: given feature
    # num_heads: head number
    # window_size: window size

    # Get dimensions
    (batch_size, seq_length, d_model) = shape(x)

    # Split into multiple heads
    Q, K, V = split_heads(x, num_heads)

    # Initialize attention output
```

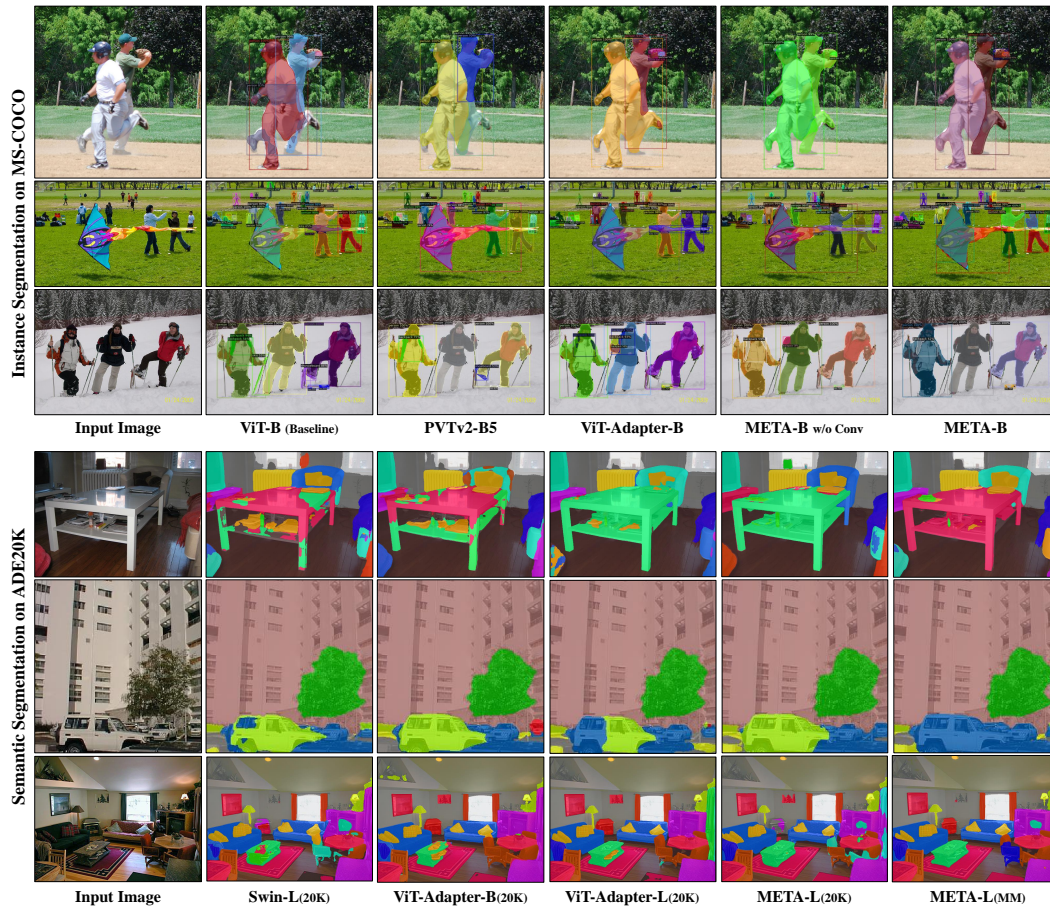


Figure 4: Qualitative results. The sample images are from the *val* set of MS-COCO (Caesar et al., 2018) for instance segmentation, and are from the *val* set of ADE20K (Zhou et al., 2017) for semantic segmentation. “w/o Conv” denotes that the Conv branch is not used in the experiments. “20K” and “MM” refers to the backbone network being pre-trained on ImageNet-22k (Steiner et al., 2021) and Multi-Modal (Zhu et al., 2022), respectively.

```

attention_output = zeros(batch_size, seq_length, d_model)

# Initialize previous head's output for cascaded attention
previous_Q = zeros(batch_size, seq_length, d_model)
previous_K = zeros(batch_size, seq_length, d_model)
previous_V = zeros(batch_size, seq_length, d_model)

# Calculate attention for each head
for head in range(num_heads):
    for position in range(seq_length):
        # Get cross-shaped window indices
        window_indices = get_cross_shaped_window_indices(position,
                                                         window_size)

        # Gather Q, K, V for the current window
        Q_window = gather(Q[head], window_indices)
        K_window = gather(K[head], window_indices)
        V_window = gather(V[head], window_indices)

        # Incorporate previous head's output for cascaded attention
        if head > 0:
            Q_window += previous_Q

```

```

        K_window += previous_K
        V_window += previous_V

        # Calculate attention scores
        attention_scores = softmax(Q_window * K_window^T / sqrt(d_k))

        # Compute the attention output for the current position
        attention_output[position] = attention_scores * V_window

        # Update previous head's output for the next head
        previous_Q = Q_window
        previous_K = K_window
        previous_V = V_window

        # Final linear transformation
        attention_output = linear_transform(attention_output)
    return attention_output

function feed_forward_network(x):
    # Feed Forward Network
    x = ReLU(linear(x))
    x = linear(x)
    return x

```

```

def get_cross_shaped_window_indices(position, window_size, seq_length):
    # Initialize the list of indices
    indices = []

    # Add the current position
    indices.append(position)

    # Add vertical neighbors (up and down)
    for offset in range(-window_size, window_size + 1):
        if position + offset >= 0 and position + offset < seq_length:
            indices.append(position + offset)

    # Remove duplicates and sort the indices
    indices = list(set(indices))
    indices.sort()

    return indices

```